JACS
JOURNAL OF THE AMERICAN CHEMICAL SOCIETY
Article
pubs.acs.org/JACS

Vacuum-Deposited Small-Molecule Organic Solar Cells with High Power Conversion Efficiencies by Judicious Molecular Design and Device Optimization

Yi-Hong Chen,[†,#] Li-Yen Lin,[‡,#] Chih-Wei Lu,[†] Francis Lin,[‡] Zheng-Yu Huang,[†] Hao-Wu Lin,*[,†] Po-Han Wang,[‡] Yi-Hung Liu,[‡] Ken-Tsung Wong,*[,‡] Jianguo Wen,[§] Dean J. Miller,[§] and Seth B. Darling[∥,⊥]

[†]Department of Materials Science and Engineering, National Tsing Hua University, Hsin Chu 30013, Taiwan

[‡]Department of Chemistry, National Taiwan University, Taipei 10617, Taiwan

[§]Electron Microscopy Center and Materials Science Division and [∥]Center for Nanoscale Materials, Argonne National Laboratory, Lemont, Illinois 60439, United States

[⊥]Institute for Molecular Engineering, The University of Chicago, Chicago, Illinois 60637, United States

Supporting Information

ABSTRACT: Three new tailor-made molecules (**DPDCTB**, **DPDCPB**, and **DTDCPB**) were strategically designed and convergently synthesized as donor materials for small-molecule organic solar cells. These compounds possess a donor−acceptor−acceptor molecular architecture, in which various electron-donating moieties are connected to an electron-withdrawing dicyanovinylene moiety through another electron-accepting 2,1,3-benzothiadiazole block. The molecular structures and crystal packings of **DTDCPB** and the previously reported **DTDCTB** were characterized by single-crystal X-ray crystallography. Photophysical and electrochemical properties as well as energy levels of this series of donor molecules were thoroughly investigated, affording clear structure−property relationships. By delicate manipulation of the trade-off between the photovoltage and the photocurrent via molecular structure engineering together with device optimizations, which included fine-tuning the layer thicknesses and the donor:acceptor blended ratio in the bulk heterojunction layer, vacuum-deposited hybrid planar-mixed heterojunction devices utilizing **DTDCPB** as the donor and C_{70} as the acceptor showed the best performance with a power conversion efficiency (PCE) of 6.6 ± 0.2% (the highest PCE of 6.8%), along with an open-circuit voltage (V_{oc}) of 0.93 ± 0.02 V, a short-circuit current density (J_{sc}) of 13.48 ± 0.27 mA/cm^2, and a fill factor (FF) of 0.53 ± 0.02, under 1 sun (100 mW/cm^2) AM 1.5G simulated solar illumination.

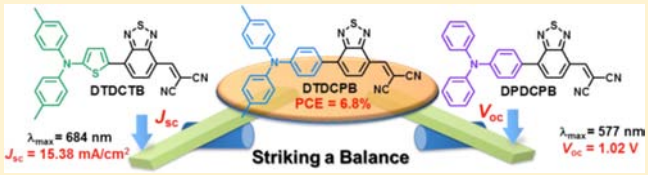

INTRODUCTION

Organic solar cells (OSCs) are under intensive interdisciplinary investigation in both academia and industry worldwide because of their potential to enable mass production of cost-effective and flexible solar energy conversion devices.[1] Over the past decade, most research efforts have focused on solution-processed polymer bulk heterojunction (BHJ) solar cells based on a blend of p-type polymers and n-type soluble fullerene derivatives as the active layer.[2] Significant progress has been made in this field, primarily stemming from combined improvements in material design,[3] morphology control,[4] interface modification,[5] and device engineering.[6] To date, power conversion efficiencies (PCEs) in the range of 6−8% have been steadily achieved for solution-processed single polymer BHJ solar cells.[5e,6e,f,7] In particular, a series of semiconducting polymeric donors (i.e., PTBs) composed of alternating benzodithiophene and ester-substituted thieno[3,4-*b*]thiophene units, developed by Yu et al., represents the most successful example, and the BHJ devices based on PTB7 blended with [6,6]-phenyl-C_{71}-butyric acid methyl ester ($PC_{71}BM$) as the acceptor have reached PCEs of up to 7.4%.[7e] Furthermore, a remarkable PCE of 8.37% has been reported for a PTB7-based device by incorporating a thin layer of alcohol/water-soluble polymer as a cathode interlayer.[5d]

In contrast, small-molecule organic solar cells (SMOSCs) featuring small molecules as donor materials have received less attention due to their inferior performance as compared to that of solution-processed polymer BHJ solar cells. However, SMOSCs are still of great interest to the research community because of the attractive advantages of small-molecule semiconductors, including well-defined molecular structures, easier purification, amenability to large-scale production, and better batch-to-batch reproducibility. As such, ever-increasing research endeavors have been dedicated to developing SMOSCs over the past few years, and efficiencies have steadily improved.[8−10] A PCE of 7% has been realized for solution-processed SMOSCs through the rational molecular design of a donor molecule and

Received: February 25, 2012
Published: July 26, 2012

dx.doi.org/10.1021/ja301872s | *J. Am. Chem. Soc.* 2012, 134, 13616−13623

a particular active-layer processing method.[9n] In addition, small-molecule semiconductors can also be fabricated by vacuum deposition due to their low molecular weight. One notable merit of vacuum-deposited SMOSCs is that multilayer tandem cells can be easily prepared;[11] these may constitute one of the promising approaches to breaking through the 10% theoretical limit for single OSCs.[12] In this context, an exceptionally high PCE of 10.7% has been released for a tandem device by Heliatek GmbH.[13] Although the performance for single SMOSCs still lags behind those of single solution-processed polymer solar cells, the current rapid advances have clearly demonstrated that they can compete with their polymeric counterparts. With regard to the structural design for molecular donors, the symmetrical quadrupolar systems[9] represent the most ubiquitous molecular scaffolds and have successfully demonstrated excellent photovoltaic performance with PCEs of up to 6.9%.[9m] In contrast, the asymmetric dipolar push−pull systems are relatively less explored,[10] among which the merocyanine dyes[10c−h] have been investigated in depth by the Würthner and Meerholz research groups. The corresponding vacuum-processed devices have shown remarkable PCEs of up to 6.1%.[10g] From our previous study of dye-sensitized solar cells, we learned that organic dyes with a donor−acceptor−acceptor (D-A-A) molecular configuration possess both a smaller bandgap and lower highest occupied molecular orbital (HOMO) level than their analogs.[14] Consequently, we argued that such D-A-A-type molecules could show the potential to concurrently enhance the short-circuit current density (J_{sc}) and open-circuit voltage (V_{oc}), as utilized as donors for SMOSCs. Along these lines, we recently reported two D-A-A-type donor molecules, **DTDCTB** and **DTDCTP**, in which an electron-donating ditolylaminothienyl moiety was connected to an electron-withdrawing dicyanovinylene (DCV) moiety through another electron-accepting 2,1,3-benzothiadiazole (BT) and pyrimidine block, respectively (Scheme 1).[15] In practical

Scheme 1. Molecular Structures of D-A-A Donors DTDCTB and DTDCTP

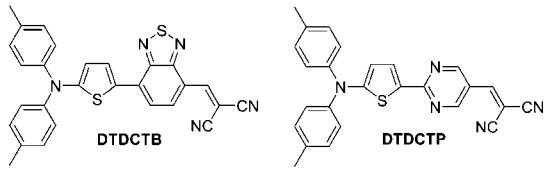

photovoltaic characterization, vacuum-deposited hybrid planar-mixed heterojunction (PMHJ) devices based on **DTDCTB** and **DTDCTP** as the donor and C_{70} as the acceptor exhibited PCEs as high as 5.81%[15a] and 6.4%,[15b] respectively. In addition, our study also revealed that the bandgaps and HOMO levels of D-A-A-type molecules can be easily fine-tuned through structural modification of their donor moieties, where their HOMOs are mainly populated, and thereby, alteration of donor moieties has a significant impact on the HOMO level but a limited effect on the LUMO level.[14] Accordingly, we envisioned that the PCEs of SMOSCs adopting our D-A-A molecules as donors could be further enhanced through delicately manipulating a trade-off between an extended spectral coverage (giving J_{sc}) and an augmented energy offset between the HOMO level of the donor and the LUMO level of the acceptor (giving V_{oc}). In this work, three new donor molecules (**DPDCTB**, **DPDCPB**, and **DTDCPB**; Scheme 2) were

Scheme 2. Synthetic Route for D-A-A Donors DPDCTB, DTDCTB, DPDCPB, and DTDCPB

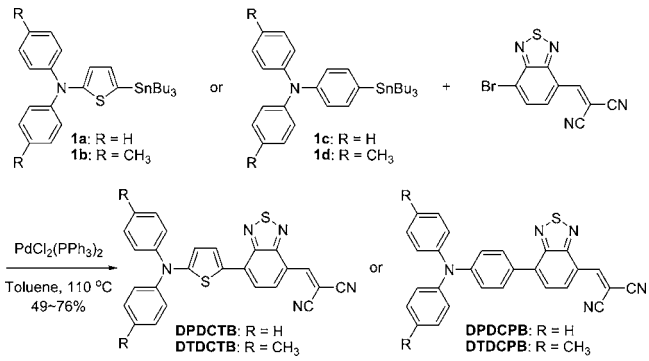

synthesized, in which the ditolylaminothienyl donor moiety of **DTDCTB** was respectively replaced by three relatively weaker electron-donating groups. The properties of this series of donor molecules (including **DTDCTB**) were investigated, and their photovoltaic performance was comprehensively studied and optimized. Remarkably, vacuum-deposited PMHJ devices utilizing **DTDCPB** as the donor and C_{70} as the acceptor gave a PCE of 6.6 ± 0.2%, with the highest PCE of up to 6.8%.

RESULTS AND DISCUSSION

The synthesis of the four donor molecules is depicted in Scheme 2. With the key asymmetric building block, 4-bromo-7-dicyanovinyl-2,1,3-benzothiadiazole, which was previously described,[15a] all target compounds were convergently prepared in gram quantities and moderate yields through Stille coupling reactions with triarylamine-based tributylstannyl derivatives **1**.

Thermal stabilities and morphological properties of these compounds were investigated by thermogravimetric analysis (TGA) and differential scanning calorimetry (DSC), respectively. The decomposition temperatures (T_d) (referring to 5% weight loss) were in the range of 279−316 °C (Table 1), indicating good thermal stability, which is an important prerequisite for device fabrication via vacuum deposition. In DSC, a melting transition manifested from one sharp endothermic peak was observed for each compound (Table 1).

The molecular structures and crystal packings of **DTDCTB** and **DTDCPB** were characterized by single-crystal X-ray crystallography (Figure 1). Suitable crystals for X-ray analyses were obtained by slow diffusion of orthogonal solvents (dichloromethane/hexane or methanol). In contrast to **DTDCTB**, which displayed an almost coplanar conformation between the thiophene and BT rings with a dihedral angle of 5.5°, **DTDCPB** was highly distorted from planarity with a dihedral angle between the phenylene and BT rings of 24.7°, due to the presence of ortho−ortho steric interactions. The highly polar nature of the heteroaryl components leads both molecules to pack in an antiparallel manner and self-assemble into centrosymmetric dimers. Such a supramolecular arrangement is similar to those observed in some highly dipolar dyes reported by Würthner and Meerholz et al. and has been proposed to effectively eliminate molecular dipole moments in the solid state and, thus, avoid the large energetic disorder that is thought to be detrimental to efficient charge carrier transport.[10c−h] The average distance between two neighboring BT rings was smaller for **DTDCTB** (ca. 3.4 Å) than for **DTDCPB** (ca. 3.5 Å), accordingly, resulting in a denser

dx.doi.org/10.1021/ja301872s | J. Am. Chem. Soc. 2012, 134, 13616−13623

Table 1. Photophysical, Electrochemical, and Thermal Parameters for DPDCTB, DTDCTB, DPDCPB, and DTDCPB

compd	λ_{abs} soln (nm)[a] (ε, M^{-1} cm^{-1})	λ_{abs} film (nm)[b]	ΔE^{opt} film (eV)[c]	E_{ox}^{1} (V)[d]	E_{red}^{1} (V)[e]	ΔE^{CV} (eV)[f]	HOMO (eV)[g]	LUMO (eV)[h]	T_d (°C)[i]	T_m (°C)[j]
DPDCTB	639 (35856)	670	1.91	0.41	−1.07	1.48	−5.35	−3.44	314	187
DTDCTB	663 (41660)	684	1.86	0.35	−1.09	1.44	−5.30	−3.44	316	234
DPDCPB	549 (24365)	577	2.14	0.60	−1.13	1.73	−5.50	−3.36	279	208
DTDCPB	570 (27445)	595	2.08	0.47	−1.19	1.66	−5.43	−3.35	308	288

[a]Measured in dichloromethane solutions (10^{-5} M). [b]Thin films prepared by vacuum deposition onto fused-silica substrates. [c]Estimated from the extinction coefficient maxima of thin films (Figure 4a). [d]Measured in dichloromethane solutions with 0.1 M tetrabutylammonium hexafluorophosphate ($TBAPF_6$) as a supporting electrolyte. [e]Measured in tetrahydrofuran solutions with 0.1 M tetrabutylammonium perchlorate (TBAP) as a supporting electrolyte. [f]Calculated from the difference between E_{ox}^{1} and E_{red}^{1}. [g]Determined by UPS. [h]LUMO = HOMO + ΔE^{opt} film. [i]Temperature corresponding to 5% weight loss obtained from TGA analysis. Under N_2 at a heating rate of 10 °C/min. [j]Temperature obtained from DSC analysis. Under N_2 at a heating rate of 10 °C/min.

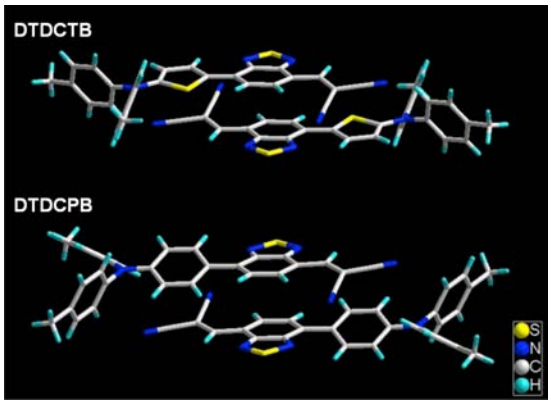

Figure 1. X-ray-determined molecular structures and crystal packings of **DTDCTB** and **DTDCPB**.

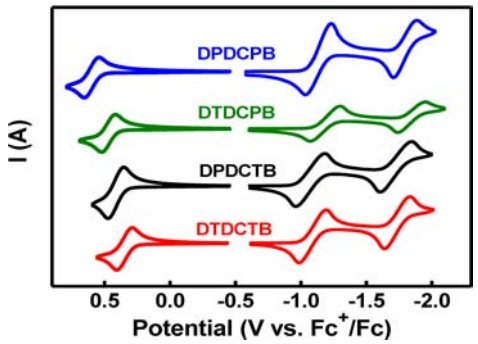

Figure 2. Cyclic voltammograms of **DPDCPB**, **DTDCPB**, **DPDCTB**, and **DTDCTB** recorded in solution.

packing [d = 1.364 g/cm^3 for **DTDCTB** vs 1.308 g/cm^3 for **DTDCPB**, Table S1 in the Supporting Information (SI)]. The degree of bond length alteration (BLA), calculated as the difference between the bond length of C4−C5 and the average bond length of C3−C4 and C5−C6 of the invariable BT acceptor, amounted to 0.001 Å for **DTDCTB** and 0.030 Å for **DTDCPB** (Table S2). The bond length between the triarylamine donors and the BT acceptor (i.e., bond length of C6−C7) for **DTDCTB** was shorter than that for **DTDCPB** (1.434 Å vs 1.472 Å). The smaller BLA of the BT acceptor and the shorter bond length of C6−C7 for **DTDCTB** indicate that the incorporation of thiophene at the donor moiety facilitates π-electron delocalization and imparts an enhanced quinoidal character to the conjugated backbone. In other words, the adoption of the ditolylaminothienyl donor moiety promotes efficient intramolecular charge transfer (ICT) from the donor side to the acceptor side of **DTDCTB**, thus leading to the formation of mesomeric structures (D−A ↔ D^+=A^-).[3a,16]

Figure 2 shows the cyclic voltammograms of the four donor molecules recorded in solution. Pertinent electrochemical data are summarized in Table 1. All four molecules exhibited one quasi-reversible oxidation wave corresponding to the oxidation of the diarylaminothienyl or diarylaminophenyl donor moieties. The less-positive oxidation potentials of **DTDCPB** and **DTDCTB** relative to **DPDCPB** and **DPDCTB** can be rationally ascribed to the presence of the stronger electron-donating *p*-tolyl substituents, while **DPDCTB** and **DTDCTB** showed less positive oxidation potentials than **DPDCPB** and **DTDCPB** due to the electron-rich nature of thiophene. On the other hand, two reversible reduction waves were observed in the cathodic potential regime. The first wave can be assigned to the reduction of the DCV block, whereas the second wave can be attributed to the reduction of the BT fragment. In contrast to the oxidation behaviors, the reduction potentials of these four molecules were relatively insensitive to the structural variations of the donor moieties, even though the reduction potentials of **DPDCTB** and **DTDCTB** were slightly less negative than those of **DPDCPB** and **DTDCPB**. Furthermore, the solid-state thin-film HOMO levels of the four molecules were determined using ultraviolet photoelectron spectroscopy (UPS) (Figure S1). The HOMO and corresponding calculated LUMO levels are summarized in Table 1. The trend observed in the HOMO levels was in good agreement with that of the oxidation potentials. Specifically, the donors bearing *p*-tolyl substituents and/or thiophene showed less positive oxidation potentials and possessed higher-lying HOMO levels than their counterparts. Apparently, the HOMO levels of our D-A-A-type molecules can be strategically fine-tuned through structural modification of the donor moieties, and solar cell devices based on these three new donors are anticipated to offer higher V_{oc} values than that of the **DTDCTB**-based device (*vide infra*).

The UV−vis absorption spectra of the four molecules in dichloromethane are depicted in Figure 3a. All showed an intense and broad absorption band in the long-wavelength region, which was assigned to the ICT transition. Compared to **DPDCPB** and **DTDCPB**, significant bathochromic shifts in absorption bands together with increases in molar extinction coefficients (ε) were found for **DPDCTB** and **DTDCTB** because of the electron-rich and fortified quinoidal characters of thiophene as well as the coplanar conformation between the thiophene and BT rings, which are all beneficial in lowering the energy and augmenting the oscillator strength of the ICT transition. In addition, the absorption peaks of **DTDCPB** and **DTDCTB** were red-shifted by ca. 20 nm as compared to those

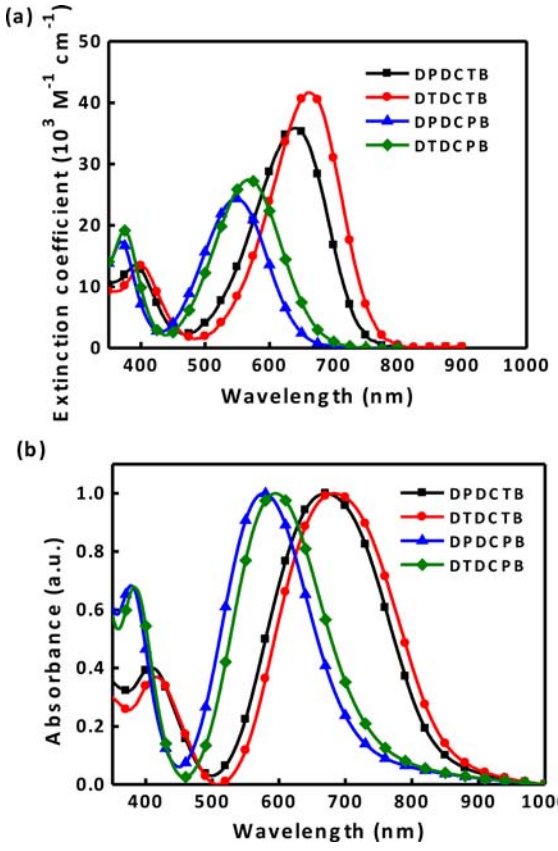

Figure 3. Absorption spectra of **DPDCTB** (squares), **DTDCTB** (circles), **DPDCPB** (triangles), and **DTDCPB** (diamonds) (a) in dichloromethane solutions and (b) as vacuum-deposited thin films.

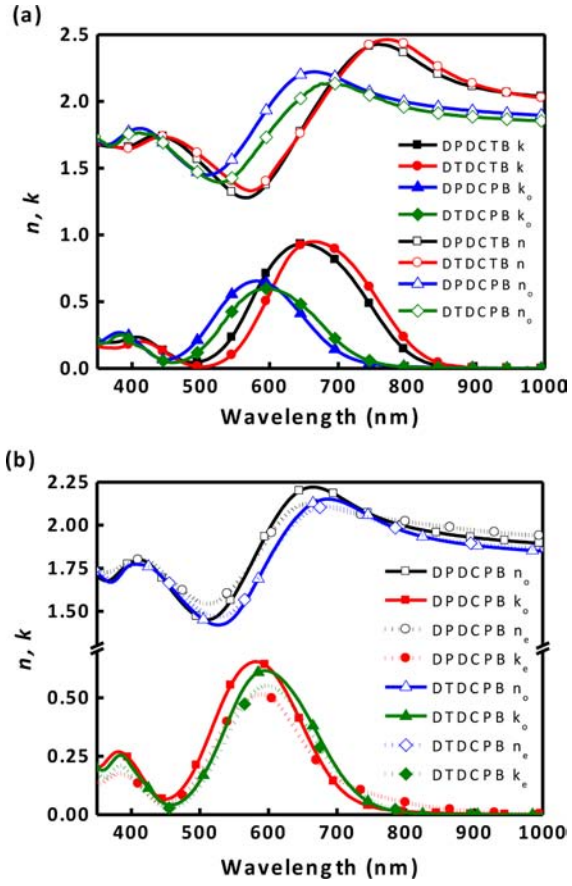

Figure 4. (a) Optical constants of **DPDCTB** (squares), **DTDCTB** (circles), **DPDCPB** (triangles), and **DTDCPB** (diamonds) thin-film spectra. (b) Ordinary (in-plane) and extraordinary (out-of-plane) optical constants of **DPDCPB** and **DTDCPB** thin-film spectra.

of **DPDCPB** and **DPDCTB** by virtue of the stronger electron-donating nature of the *p*-tolyl substituents. On the other hand, the thin-film absorption bands of these molecules were broadened and red-shifted in comparison to those observed in solution (Figure 3b), likely due to the intermolecular $\pi-\pi$ stacking of the molecules in the solid state as manifested in the crystal packings.

Optical constants (refractive index, n, and extinction coefficient, k) of vacuum-deposited thin films of the four molecules, determined by the combination of reflection and transmission ellipsometry, are shown in Figure 4a.[17] The trend in the maximum extinction coefficients is well coincident with that in the absorption maxima. Both **DPDCTB** and **DTDCTB** thin films can be modeled as isotropic layers and show high k_{max} values of ~1 that are among the highest reported for organic solar-active materials.[18] However, the optical isotropic model cannot be adopted to describe the behavior of the two phenylene-containing molecules (**DPDCPB** and **DTDCPB**) thin-films. Therefore, the **DPDCPB** and **DTDCPB** films were treated as uniaxially anisotropic with the optical axis along the surface normal. That means the optical constants are distinguished by those for the ordinary (in-plane) polarization, $n_o + ik_o$ and those for the extraordinary (out-of-plane) polarization, $n_e + ik_e$.[17] The uniaxial model can be successfully fitted to the experimental data, and the extracted optical constants are shown in Figure 4b. The larger k_o relative to k_e for **DPDCPB** and **DTDCPB** indicates preferred orientations parallel to the surface plane upon vacuum deposition onto substrates, as the transition dipole moment of the lowest energy excited state is usually along the molecular backbone for molecules with linear π-systems.[17] This uniaxial anisotropy property generally contributes to stronger absorption for horizontally polarized incident light and therefore may favor high J_{sc} (*vide infra*).[19]

In common with the photovoltaic characterization of **DTDCTB**,[15a] the vacuum-deposited PMHJ structure was adopted in this study,[8a,c] where the active layers were composed of a BHJ layer sandwiched between a homogeneous donor and acceptor layer. This kind of device architecture can provide not only efficient photon harvesting but also good photogenerated charge carrier transport to the respective electrodes. Fullerene C_{70} was chosen as the electron-accepting counterpart owing to its broader and larger extinction coefficients relative to C_{60}. More importantly, the C_{70}-based PMHJ devices always demonstrated higher PCEs than C_{60}-based PMHJ devices in our previous investigations.[15,19,20] Generally, the devices were fabricated with a configuration of ITO/MoO_3 (5 nm)/donor (7 nm)/donor:C_{70}/C_{70} (7 nm)/2,9-dimethyl-4,7-diphenyl-1,10-phenanthroline (BCP) (10 nm)/Ag (150 nm). In these devices, the MoO_3 thin film acts as the hole-transporting layer, and the BCP thin film serves as the electron-transporting layer with an exciton blocking character. The optimal thicknesses of the active layers (the donor layer, donor:C_{70} BHJ layer, and C_{70} layer) are dependent on the optical field distribution as well as exciton diffusion lengths and carrier recombination rates in the thin films.[15] Practical devices with various thicknesses for active layers were fabricated and

dx.doi.org/10.1021/ja301872s | J. Am. Chem. Soc. 2012, 134, 13616−13623

measured. The optimized thicknesses of the BHJ layer in **DPDCTB**-, **DTDCTB**-, **DPDCPB**-, and **DTDCPB**-based devices were found to be 50, 40, 40, and 40 nm, respectively. In addition, the donor:C_{70} blended volume ratio in the BHJ layer was also systematically fine-tuned (Figure S2−5 and Table S3−6). The devices fabricated with a donor:C_{70} ratio of 1:1.6 in the BHJ layer gave the best results, except for the **DPDCPB**:C_{70} device that showed the best performance at a ratio of 1:1.

Device performance measurements were carried out under ambient atmosphere using 100 mW/cm^2 AM 1.5G simulated solar illumination. Spectral mismatch-corrected current density−voltage (J−V) characteristics of the donor:C_{70} (1:1.6) and **DPDCPB**:C_{70} (1:1) PMHJ devices are shown in Figure 5a, and

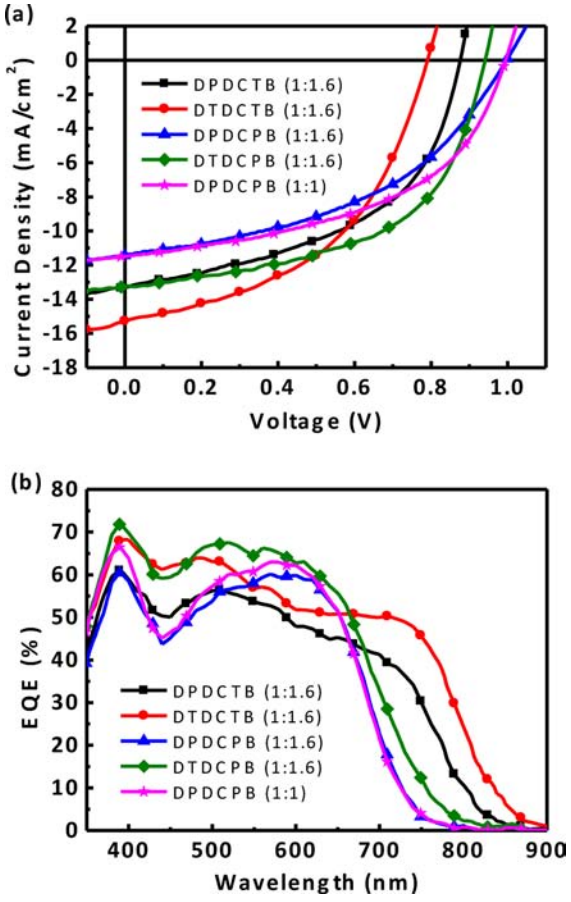

Figure 5. (a) Mismatch-corrected J−V characteristics (under 1 sun, AM 1.5G illumination) and (b) EQE spectra of **DPDCTB**:C_{70} (1:1.6) (squares), **DTDCTB**:C_{70} (1:1.6) (circles), **DPDCPB**:C_{70} (1:1.6) (triangles), **DTDCPB**:C_{70} (1:1.6) (diamonds), and **DPDCPB**:C_{70} (1:1) (stars) PMHJ solar cells.

the corresponding solar cell characteristics derived from these curves are summarized in Table 2.[21] As expected, the V_{oc} values obtained in these devices are consistent with the magnitudes of the HOMO levels of the donors in spite of the various donor:C_{70} blended ratios. The **DPDCPB**:C_{70} device gave a maximum V_{oc} value of 1.00 ± 0.02 V, reflecting the fact that **DPDCPB** possesses the lowest HOMO level. Moreover, the differences in V_{oc} values were closely correlated to those in the HOMO levels. On the other hand, the J_{sc} values generally followed the trend in donor bandgaps, with a maximum value of 15.08 ± 0.30 mA/cm^2 generated in the **DTDCTB**:C_{70} (1:1.6) device, which was among the highest values ever reported for OSCs. Interestingly, the J_{sc} value of the **DPDCTB**:C_{70} device was slightly lower than that of the **DTDCPB**:C_{70} device, even though **DPDCTB** exhibited larger extinction coefficients and a smaller band gap than those of **DTDCPB**, which can possibly be attributed to beneficial impact from the uniaxial anisotropy character of **DTDCPB**. The external quantum efficiency (EQE) spectra of the PMHJ solar cells, shown in Figure 5b, were used to calculate the mismatch factors.[21] Both EQE spectra of the **DPDCTB**:C_{70} and **DTDCTB**:C_{70} devices exhibited high plateaus of ∼50% (or even higher) throughout the UV−vis range and extend to the near-IR region, whereas the **DTDCPB**:C_{70} cell delivered the highest EQEs over the UV−vis range among this series of devices. The calculated J_{sc} values obtained by integrating the EQE spectra with the standard AM 1.5G solar spectrum matched the measured J_{sc} values within 3−5%. It is worthwhile to mention that the structural modulation of the donor moieties in these D-A-A donors and consequent shift of their HOMO levels and adjustment of their bandgaps clearly lead to a trade-off between the V_{oc} and J_{sc} values. Remarkably, the **DTDCPB**:C_{70} device exhibited the best performance through striking a balance between the photovoltage and photocurrent, thus resulting in a PCE of 6.6 ± 0.2% (the highest of 6.8%) with a V_{oc} of 0.93 ± 0.02 V, J_{sc} of 13.48 ± 0.27 mA/cm^2, and fill factor (FF) of 0.53 ± 0.02. The **DTDCPB**:C_{70} (1:1.6) device was certified by the Photovoltaic Metrology Laboratory, Industrial Technology Research Institute (ITRI) to have a PCE of 6.68% (see certification report in SI).

To gain insight into the differences in the performance of **DTDCPB**:C_{70} PMHJ devices at various blended ratios, carrier mobilities and thin film morphologies were examined. The carrier mobilities were measured using the space charge-limited current (SCLC) method. The hole and electron mobilities for the **DTDCPB**:C_{70} (1:1.6) blended film were 6.49×10^{-5} and 4.32×10^{-4} cm^2 V^{-1} s^{-1} at 700 (V/cm)$^{0.5}$, respectively, which were higher and more balanced than those for the **DTDCPB**:C_{70} (1:1) film (Figure S6 and Table S7), thus contributing to the higher device performance for the **DTDCPB**:C_{70} (1:1.6) device. Although significant achievements have already been realized in our system, further improvements in PCEs are still in high demand. In this respect, the moderate FF values of ∼0.5 obtained in our devices represent a potential area for further optimization to obtain even better performance. Specifically, the shunt resistances (R_{shunt}) in our devices, calculated from the inverse slopes of the J−V curves in the fourth quadrant, are several orders of magnitude lower than those in optimized polymer solar cells (Table 2).[4b,22] In general, both a high R_{shunt} and a low series resistance (R_{series}) are desirable for producing high FF, and a low R_{shunt} actually stems from more charge recombination and leakage current.[23] Accordingly, increasing hole mobility and thus realizing more balanced carrier transport, to improve the R_{shunt} and the resulting FF values, will be a future research focus.[24]

To extract more information from the BHJ layer, surface morphologies of the donor:C_{70} (1:1.6) and **DPDCPB**:C_{70} (1:1) blended films were analyzed by tapping-mode atomic force microscopy (AFM). Although the AFM images revealed the existence of phase separation (Figure S7), there were no decisive variations useful to account for the achieved device performance. Therefore, transmission electron microscopy (TEM) and scanning transmission electron microscopy

dx.doi.org/10.1021/ja301872s | J. Am. Chem. Soc. 2012, 134, 13616−13623

Table 2. Photovoltaic Parameters of PMHJ Solar Cells under AM 1.5G Simulated Solar Illumination at an Intensity of 100 mW/cm^2

device type	J_{sc} (mA/cm^2)	V_{oc} (V)	FF	PCE [highest] (%)	R_{series} (Ω·cm^2)	R_{shunt} (Ω·cm^2)
DPDCTB:C_{70} (1:1.6)	12.99 ± 0.42	0.88 ± 0.02	0.49 ± 0.01	5.6 ± 0.2 [5.8]	8.3	234.5
DTDCTB:C_{70} (1:1.6)	15.08 ± 0.30	0.79 ± 0.02	0.48 ± 0.01	5.7 ± 0.1 [5.8]	13.5	187.0
DPDCPB:C_{70} (1:1.6)	11.28 ± 0.29	1.00 ± 0.02	0.45 ± 0.02	5.0 ± 0.1 [5.1]	27.0	322.8
DTDCPB:C_{70} (1:1.6)	13.48 ± 0.27	0.93 ± 0.02	0.53 ± 0.02	6.6 ± 0.2 [6.8]	10.6	413.0
DPDCTB:C_{70} (1:1)	12.56 ± 0.45	0.85 ± 0.02	0.42 ± 0.02	4.5 ± 0.2 [4.7]	19.8	174.6
DTDCTB:C_{70} (1:1)	14.72 ± 0.25	0.79 ± 0.02	0.49 ± 0.01	5.7 ± 0.1 [5.8]	7.9	205.9
DPDCPB:C_{70} (1:1)	11.45 ± 0.23	1.00 ± 0.02	0.49 ± 0.01	5.5 ± 0.1 [5.6]	15.4	396.3
DTDCPB:C_{70} (1:1)	12.72 ± 0.40	0.92 ± 0.02	0.53 ± 0.01	6.2 ± 0.2 [6.4]	12.5	418.8

(STEM) were applied to provide morphological information for the **DTDCPB**:C_{70} (1:1) and (1:1.6) blended films. STEM high-angle annular dark-field (HAADF) imaging revealed contrast variations in both the **DTDCPB**:C_{70} (1:1.6) and (1:1) films (shown in Figure S8), even though the morphological details were markedly different between these samples. The 1:1 blend sample exhibited a less distinctly resolved domain structure and smaller features compared with the 1:1.6 system. The lower PCE of the 1:1 device may be due to inferior charge-transport pathways as a result of discontinuous domain structures through the active layer thickness, which is expected to result in increased nongeminate charge carrier recombination.[25] Ongoing studies are aimed at deciphering the spatially resolved composition of the domains, which will likely result in new insights into the photovoltaic processes in these materials.

CONCLUSIONS

In summary, three new D-A-A-type donor molecules (**DPDCTB**, **DPDCPB**, and **DTDCPB**) with various donor moieties were synthesized in a facile fashion by taking advantage of the asymmetric building block, 4-bromo-7-dicyanovinyl-2,1,3-benzothiadiazole. X-ray structure analyses revealed the tendency of these highly dipolar molecules to pack in an antiparallel manner and self-assemble into centrosymmetric dimers in the solid state. The adoption of thiophene-based donors facilitated π-electron delocalization and the formation of quinoidal mesomeric structures over the conjugated backbone. Compared to **DTDCTB,** bearing the strongest ditolylaminothienyl donor moiety among this series of molecules, the three new molecules possessed lower HOMO levels and exhibited hypsochromic shifts in absorption. Through judicious molecular design and device optimizations, including fine-tuning the layers' thicknesses as well as the blended ratio in the BHJ layer, vacuum-deposited PMHJ devices based on this series of molecules as donors and C_{70} as the acceptor showed PCEs in excess of 5.6%. Notably, the **DTDCPB**-based devices achieved an impressively high PCE of 6.8% through striking a balance between the photovoltage and the photocurrent. We believe that our molecular design concept paves a new avenue for developing high-performance donor materials for SMOSCs. Further engineering of molecular structures and morphology optimization, such as substrate heating and postannealing in order to boost device efficiencies,[26] are currently underway.

EXPERIMENTAL SECTION

Synthesis and Materials. All chemicals and reagents were used as received from commercial sources without purification. Solvents for chemical synthesis were purified by distillation. All chemical reactions were carried out under an argon or nitrogen atmosphere.

Synthesis of 2-{[7-(4-*N*,*N*-ditolylaminophenylen-1-yl)-2,1,3-benzothiadiazol-4-yl]methylene}malononitrile (DTDCPB). A mixture of 4-bromo-7-dicyanovinyl-2,1,3-benzothiadiazole (3.49 g, 12 mmol), 4-(*N*,*N*-ditolylamino)-1-(tri-*n*-butylstannyl)phenylene (**1d**) (8.1 g, 14.4 mmol), and $PdCl_2(PPh_3)_2$ (421 mg, 0.6 mmol) in anhydrous toluene (60 mL) was stirred and heated to 110 °C under argon for 5 h. After the reaction mixture was cooled to room temperature, the solvent was removed by rotary evaporation, and the crude product was purified by column chromatography on silica gel with dichloromethane/hexane (v/v, 4:3) as eluent, to afford **DTDCPB** as a black solid (4.43 g, 76%), mp 288 °C (DSC); IR (KBr) ν: 3031, 2918, 2858, 2218, 1592, 1505, 1471, 1328, 1264, 1189, 1102, 946, 826 cm^{-1}; ^{1}H NMR ($CDCl_3$, 400 MHz, δ) 8.82 (s, 1H), 8.78 (d, J = 7.6 Hz, 1H), 7.95 (d, J = 9.2 Hz, 2H), 7.84 (d, J = 7.6 Hz, 1H), 7.15−7.09 (m, 10H), 2.36 (s, 6H); ^{13}C NMR ($CDCl_3$, 100 MHz, δ) 154.4, 152.6, 152.5, 150.0, 143.9, 140.0, 134.0, 130.7, 130.4, 130.0, 127.3, 125.7, 125.5, 121.1, 120.1, 113.9, 113.1, 81.8, 21.1; HRMS-FAB$^+$ (m/z): calcd for $C_{30}H_{21}N_5S$, 483.1518; found, 483.1516.

Synthesis of 2-{[7-(5-*N*,*N*-diphenylaminothiophen-2-yl)-2,1,3-benzothiadiazol-4-yl]methylene}malononitrile (DPDCTB). The synthetic procedure was similar to that of **DTDCPB**, except that the eluent for column purification was dichloromethane/hexane (v/v, 1:1). **DPDCTB** was isolated as a black solid (63%), mp 187 °C (DSC); IR (KBr) ν: 3034, 2218, 1579, 1532, 1487, 1296, 1059, 756 cm^{-1}; ^{1}H NMR ($CDCl_3$, 400 MHz) δ 8.69 (s, 1H), 8.64 (d, J = 8.0 Hz, 1H), 8.22 (d, J = 4.0 Hz, 1H), 7.65 (d, J = 8.0 Hz, 1H), 7.40−7.36 (m, 4H), 7.32−7.29 (m, 4H), 7.21 (t, J = 7.2 Hz, 2H), 6.61 (d, J = 4.0 Hz, 1H); ^{13}C NMR ($CDCl_3$, 100 MHz) δ 159.7, 154.5, 151.7, 150.7, 146.4, 133.7, 132.5, 130.8, 129.6, 127.3, 125.3, 124.7, 121.5, 119.4, 116.2, 114.4, 113.6, 79.4; HRMS-FAB$^+$ (m/z): calcd for $C_{26}H_{15}N_5S_2$, 461.0769; found, 461.0760.

Synthesis of 2-{[7-(4-*N*,*N*-diphenylaminophenylen-1-yl)-2,1,3-benzothiadiazol-4-yl]methylene}malononitrile (DPDCPB). The synthetic procedure was similar to that of **DTDCPB**, except that the eluent for column purification was dichloromethane/hexane (v/v, 1:1). **DPDCPB** was isolated as a black solid (49%), mp 208 °C (DSC); IR (KBr) ν: 3047, 2223, 1584, 1524, 1474, 1370, 1336, 1270, 1192, 1044, 931, 821 cm^{-1}; ^{1}H NMR ($CDCl_3$, 400 MHz) δ 8.83 (s, 1H), 8.79 (d, J = 7.6 Hz, 1H), 7.98 (d, J = 8.8 Hz, 2H), 7.86 (d, J = 7.6 Hz, 1H), 7.35−7.31 (m, 4H), 7.22−7.18 (m, 6H), 7.13 (t, J = 7.2 Hz, 2H); ^{13}C NMR ($CDCl_3$, 100 MHz) δ 154.4, 152.6, 152.5, 149.6, 146.6, 139.9, 130.7, 130.5, 129.4, 128.2, 125.8, 125.5, 124.2, 121.4, 121.3, 113.9, 113.1, 82.2; HRMS-FAB$^+$ (m/z): calcd for $C_{28}H_{17}N_5S$, 455.1205; found, 455.1204.

Solar Cell Fabrication and Testing. Fullerene C_{70} and BCP were subjected to purification at least once by temperature-gradient sublimation before use in this study. The organic and metal oxide thin films as well as metal electrodes were deposited on indium tin oxide (ITO)-coated glass substrates in a high-vacuum chamber with base pressure ~1 × 10^{-6} Torr. The sheet resistance of ITO was ~15 Ω/sq. The deposition was performed at a rate of 2−3 Å/s with the substrate held at room temperature. Thicknesses were monitored using a crystal oscillator during deposition and were verified later with spectroscopic ellipsometry. The active area of the cells had an average

size of 2.5 mm^2 (intersection area between Ag cathode and ITO anode) and were carefully measured device-by-device using a calibrated optical microscope. Devices were encapsulated using a UV-cured sealant (Epowide EX, Everwide Chemical Co.) and a cover glass under an anhydrous nitrogen atmosphere after fabrication and were measured in air. Current density−voltage characteristics were measured with a SourceMeter Keithley 2636A under illumination of AM 1.5G solar light from a xenon lamp solar simulator (Abet Technologies). The incident light intensity was calibrated as 100 mW/cm^2. Taking into account the spectral mismatch between the solar simulator used in this work and the AM 1.5G reference spectrum (IEC 60904) as well as the mismatch of the photoresponse spectral coverage of the reference cell (KG5-filtered Si diode) and the test cells, the mismatch factors were calculated to be 1.006 (**DPDCTB**:C_{70} (1:1.6)), 1.014 (**DTDCTB**:C_{70} (1:1.6)), 0.994 (**DPDCPB**:C_{70} (1:1.6)), 0.997 (**DTDCPB**:C_{70} (1:1.6)), and 0.993 (**DPDCPB**:C_{70} (1:1)).[21] Short-circuit current densities were all corrected by mismatch factors. The devices were measured without a mask (the J_{sc} of cells with and without a mask had been examined, and the difference was always <3% due to the low conductive hole/electron transporting layers used in this study). The deviation values were obtained from device-to-device variations of 4−8 devices. The external quantum efficiency spectra were taken by illuminating chopped monochromatic light with a continuous-wave bias white light (from a halogen lamp) on the solar cells. The photocurrent signals were extracted with a lock-in technique using a current preamplifier (Stanford Research Systems) followed by a lock-in amplifier (AMETEK). The EQE measurement was fully computer-controlled, and the intensity of the monochromatic light was calibrated with an NIST-traceable optical power meter (Ophir Optronics). Absorption spectra were acquired with a spectrometer (PerkinElmer). Organic films for photoelectron spectroscopy and ellipsometry measurements were vacuum deposited onto fused-silica substrates. The HOMO levels of molecules were acquired with a photoelectron spectrometer (Riken Keiki Co. Ltd.). Ellipsometry measurements were carried out with a J. A. Woollam Inc. V-VASE variable-angle spectroscopic ellipsometer. The anisotropic optical constants of a sample were determined by the combination of reflection and transmission ellipsometry, which in principle is simpler and eliminates the risk of sample-to-sample variation.[17] The simulation program was coded with Matlab software (The MathWorks, Inc.) and performed with a dual-core Intel-CPU personal computer. AFM images were taken with a Veeco Nanoscope 3100 atomic force microscope. For accurate comparisons, the film preparation conditions for the AFM measurements were the same as those for device fabrication. TEM samples were vacuum-deposited active films on poly(3,4-ethylenedioxythiophene): poly(styrenesulfonate) (PEDOT:PSS) precoated Si wafers, which then were transferred to holey carbon grids by dissolving the PEDOT:PSS layer in deionized water. TEM and HAADF imaging were performed on an FEI Titian TEM with a Cs and Cc image corrector developed by CEOS GmbH (Heidelberg, Germany). To study these thin films, 200 kV was used, and no obvious beam damage was observed. HAADF images were collected using an inner cutoff angle of about 70 mrad to increase scattering intensity from light elements. The electron and hole mobilities for the **DTDCPB**:C_{70} blended films were determined using the SCLC method. The hole-only device was configured as follows: ITO/MoO_3 (1 nm)/**DTDCPB**:C_{70} (100 nm)/MoO_3 (10 nm)/Al (80 nm), while the electron-only device was configured as follows: ITO/Mg (5 nm)/**DTDCPB**:C_{70} (100 nm)/Ca (5 nm)/Al (80 nm). Current density−voltage characteristics of SCLC devices were also measured with a SourceMeter Keithley 2636A.

■ ASSOCIATED CONTENT

Ⓢ Supporting Information

Crystal data and selected bond lengths for **DTDCTB** and **DTDCPB**, UPS spectra of all donors, device optimization for all donors, a mobility diagram for **DTDCPB**:C_{70} (1:1.6) and **DTDCPB**:C_{70} (1:1) blended films, calculation details of mismatch factors, certification report, AFM images for donor:C_{70} (1:1.6) and **DPDCPB**:C_{70} (1:1) blended films, TEM and STEM images for **DTDCPB**:C_{70} (1:1.6) and **DTDCPB**:C_{70} (1:1) blended films, copies of ^1H and ^{13}C NMR spectra, and CIF for **DTDCPB**. This material is available free of charge via the Internet at http://pubs.acs.org.

■ AUTHOR INFORMATION

Corresponding Author

hwlin@mx.nthu.edu.tw; kenwong@ntu.edu.tw

Author Contributions

[#]These authors contributed equally.

Notes

The authors declare no competing financial interest.

■ ACKNOWLEDGMENTS

The authors would like to acknowledge financial support from the National Science Council of Taiwan (NSC 98-2112-M-007-028-MY3, 98-2119-M-002-007-MY3) and the Low Carbon Energy Research Center, National Tsing Hua University. Use of the Electron Microscopy Center (EMC) for Materials Research and the Center for Nanoscale Materials (CNM) at Argonne National Laboratory was supported by the U.S. Department of Energy, Office of Science, Office of Basic Energy Sciences, under contract no. DE-AC02-06CH11357.

■ REFERENCES

(1) (a) Tang, C. W. *Appl. Phys. Lett.* **1986**, *48*, 183. (b) Yu, G.; Gao, J.; Hummelen, J. C.; Wudl, F.; Heeger, A. J. *Science* **1995**, *270*, 1789. (c) Krebs, F. C. *Sol. Energy Mater. Sol. Cells* **2009**, *93*, 394.

(2) (a) Thompson, B. C.; Fréchet, J. M. J. *Angew. Chem., Int. Ed.* **2008**, *47*, 58. (b) Brabec, C. J.; Gowrisanker, S.; Halls, J. J. M.; Laird, D.; Jia, S.; Williams, S. P. *Adv. Mater.* **2010**, *22*, 3839.

(3) (a) Cheng, Y.-J.; Yang, S.-H.; Hsu, C.-S. *Chem. Rev.* **2009**, *109*, 5868. (b) Wong, W.-Y.; Ho, C.-L. *Acc. Chem. Res.* **2010**, *43*, 1246. (c) Huang, F.; Chen, K.-S.; Yip, H.-L.; Hau, S. K.; Acton, O.; Zhang, Y.; Luo, J.; Jen, A. K.-Y. *J. Am. Chem. Soc.* **2009**, *131*, 13886. (d) He, Y.; Chen, H.-Y.; Hou, J.; Li, Y. *J. Am. Chem. Soc.* **2010**, *132*, 1377. (e) Zhao, G.; He, Y.; Li, Y. *Adv. Mater.* **2010**, *22*, 4355.

(4) (a) Ma, W.; Yang, C.; Gong, X.; Lee, K.; Heeger, A. J. *Adv. Mater.* **2005**, *15*, 1617. (b) Li, G.; Shrotriya, V.; Huang, J.; Yao, Y.; Moriarty, T.; Emery, K.; Yang, Y. *Nat. Mater.* **2005**, *4*, 864. (c) Li, G.; Yao, Y.; Yang, H.; Shrotriya, V.; Yang, G.; Yang, Y. *Adv. Funct. Mater.* **2007**, *17*, 1636. (d) Peet, J.; Kim, J. Y.; Coates, N. E.; Ma, W. L.; Moses, D.; Heeger, A. J.; Bazan, G. C. *Nat. Mater.* **2007**, *6*, 497.

(5) (a) Kim, J. Y.; Kim, S. H.; Lee, H.-H.; Lee, K.; Ma, W.; Gong, X.; Heeger, A. J. *Adv. Mater.* **2006**, *18*, 572. (b) Sun, Y.; Takacs, C. J.; Cowan, S. R.; Seo, J. H.; Gong, X.; Roy, A.; Heeger, A. J. *Adv. Mater.* **2011**, *23*, 2226. (c) Seo, J.-H.; Gutacker, A.; Sun, Y.; Wu, H.; Huang, F.; Cao, Y.; Scherf, U.; Heeger, A. J.; Bazan, G. C. *J. Am. Chem. Soc.* **2011**, *133*, 8416. (d) He, Z.; Zhong, C.; Huang, X.; Wong, W.-Y.; Wu, H.; Chen, L.; Su, S.; Cao, Y. *Adv. Mater.* **2011**, *23*, 4636. (e) Fan, X.; Cui, C.; Fang, G.; Wang, J.; Li, S.; Cheng, F.; Long, H.; Li, Y. *Adv. Funct. Mater.* **2012**, *22*, 585.

(6) (a) Xu, Z.; Chen, L.-M.; Yang, G.; Huang, C.-H.; Hou, J.; Wu, Y.; Li, G.; Hsu, C.-S.; Yang, Y. *Adv. Funct. Mater.* **2009**, *19*, 1227. (b) Chen, L.-M.; Hong, Z.; Li, G.; Yang, Y. *Adv. Mater.* **2009**, *21*, 1434. (c) Hsieh, C.-H.; Cheng, Y.-J.; Li, P.-J.; Chen, C.-H.; Dubosc, M.; Liang, R.- M.; Hsu, C.-S. *J. Am. Chem. Soc.* **2010**, *132*, 4887. (d) Cheng, Y.-J.; Hsieh, C.-H.; He, Y.; Hsu, C.-S.; Li, Y. *J. Am. Chem. Soc.* **2010**, *132*, 17381. (e) Chang, C.-Y.; Wu, C.-E.; Chen, S.-Y.; Cui, C.; Cheng, Y.-J.; Hsu, C.-S.; Wang, Y.-L.; Li, Y. *Angew. Chem., Int. Ed.* **2011**, *50*, 9386. (f) Small, C. E.; Chen, S.; Subbiah, J.; Amb, C. M.; Tsang, S.-W.; Lai, T.-H.; Reynolds, J. R.; So, F. *Nat. Photonics* **2012**, *6*, 115.

(7) (a) Park, S. H.; Roy, A.; Beaupre, S.; Cho, S.; Coates, N.; Moon, J. S.; Moses, D.; Leclerc, M.; Lee, K.; Heeger, A. J. *Nat. Photonics* **2009**,

3, 297. (b) Chen, Y.-C.; Yu, C.-Y.; Fan, Y.-L.; Hung, L.-I; Chen, C.-P.; Ting, C. *Chem. Commun.* **2010**, *46*, 6503. (c) Zhang, Y.; Zou, J.; Yip, H.-L.; Chen, K.-S.; Zeigler, D. F.; Sun, Y.; Jen, A. K.-Y. *Chem. Mater.* **2011**, *23*, 2289. (d) Chen, H.-Y.; Hou, J.; Zhang, S.; Liang, Y.; Yang, G.; Yang, Y.; Yu, L.; Wu, Y.; Li, G. *Nat. Photonics* **2009**, *3*, 649. (e) Liang, Y.; Xu, Z.; Xia, J.; Tsai, S.-T.; Wu, Y.; Li, G.; Ray, C.; Yu, L. *Adv. Mater.* **2010**, *22*, E135. (f) Zhou, H.; Yang, L.; Stuart, A. C.; Price, S. C.; Liu, S.; You, W. *Angew. Chem., Int. Ed.* **2011**, *50*, 2995. (g) Price, S. C.; Stuart, A. C.; Yang, L.; Zhou, H.; You, W. *J. Am. Chem. Soc.* **2011**, *133*, 4625. (h) Chu, T.-Y.; Lu, J.; Beaupre, S.; Zhang, Y.; Pouliot, J.-R.; Wakim, S.; Zhou, J.; Leclerc, M.; Li, Z.; Ding, J.; Tao, Y. *J. Am. Chem. Soc.* **2011**, *133*, 4250. (i) Huo, L.; Zhang, S.; Guo, X.; Xu, F.; Li, Y.; Hou, J. *Angew. Chem., Int. Ed.* **2011**, *50*, 9697.

(8) (a) Hiramoto, M.; Fujiwara, H.; Yokoyama, M. *Appl. Phys. Lett.* **1991**, *58*, 1062. (b) Peumans, P.; Uchida, S.; Forrest, S. R. *Nature* **2003**, *425*, 158. (c) Xue, J.; Rand, B. P.; Uchida, S.; Forrest, S. R. *Adv. Mater.* **2005**, *17*, 66. (d) Matsuo, Y.; Sato, Y.; Niinomi, T.; Soga, I.; Tanaka, H.; Nakamura, E. *J. Am. Chem. Soc.* **2009**, *131*, 16048. (e) Walker, B.; Kim, C.; Nguyen, T.-Q. *Chem. Mater.* **2011**, *23*, 470. (f) Mishra, A.; Bäuerle, P. *Angew. Chem., Int. Ed.* **2012**, *51*, 2020. (g) Lin, Y.; Li, Y.; Zhan, X. *Chem. Soc. Rev.* **2012**, *41*, 4245.

(9) (a) Walker, B.; Tamayo, A. B.; Dang, X.-D.; Zalar, P.; Seo, J. H.; Garcia, A.; Tantiwiwat, M.; Nguyen, T.-Q. *Adv. Funct. Mater.* **2009**, *19*, 3063. (b) Shang, H.; Fan, H.; Liu, Y.; Hu, W.; Li, Y.; Zhan, X. *Adv. Mater.* **2011**, *23*, 1554. (c) Loser, S.; Bruns, C. J.; Miyauchi, H.; Ortiz, R. P.; Facchetti, A.; Stupp, S. I.; Marks, T. J. *J. Am. Chem. Soc.* **2011**, *133*, 8142. (d) Wei, G.; Wang, S.; Sun, K.; Thompson, M. E.; Forrest, S. R. *Adv. Energy Mater.* **2011**, *1*, 184. (e) Lassiter, B. E.; Wei, G.; Wang, S.; Zimmerman, J. D.; Diev, V. V.; Thompson, M. E.; Forrest, S. R. *Appl. Phys. Lett.* **2011**, *98*, 243307. (f) Wei, G.; Xiao, X.; Wang, S.; Zimmerman, J. D.; Sun, K.; Diev, V. V.; Thompson, M. E.; Forrest, S. R. *Nano Lett.* **2011**, *11*, 4261. (g) Zhou, J.; Wan, X.; Liu, Y.; Long, G.; Wang, F.; Li, Z.; Zuo, Y.; Li, C.; Chen, Y. *Chem. Mater.* **2011**, *23*, 4666. (h) Li, Z.; He, G.; Wan, X.; Liu, Y.; Zhou, J.; Long, G.; Zuo, Y.; Zhang, M.; Chen, Y. *Adv. Energy Mater.* **2012**, *2*, 74. (i) Lee, O. P.; Yiu, A. T.; Beaujuge, P. M.; Woo, C. H.; Holcombe, T. W.; Millstone, J. E.; Douglas, J. D.; Chen, M. S.; Fréchet, J. M. J. *Adv. Mater.* **2011**, *23*, 5359. (j) Sun, Y.; Welch, G. C.; Leong, W. L.; Takacs, C. J.; Bazan, G. C.; Heeger, A. J. *Nat. Mater.* **2012**, *11*, 44. (k) Schulze, K.; Uhrich, C.; Schüppel, R.; Leo, K.; Pfeiffer, M.; Brier, E.; Reinold, E.; Bäuerle, P. *Adv. Mater.* **2006**, *18*, 2872. (l) Fitzner, R.; Reinold, E.; Mishra, A.; Mena-Osteritz, E.; Ziehlke, H.; Körner, C.; Leo, K.; Riede, M.; Weil, M.; Tsaryova, O.; Weiß, A.; Uhrich, C.; Pfeiffer, M.; Bäuerle, P. *Adv. Funct. Mater.* **2011**, *21*, 897. (m) Fitzner, R.; Mena-Osteritz, E.; Mishra, A.; Schulz, G.; Reinold, E.; Weil, M.; Körner, C.; Ziehlke, H.; Elschner, C.; Leo, K.; Riede, M.; Pfeiffer, M.; Uhrich, C.; Bäuerle, P. *J. Am. Chem. Soc.* **2012**, *134*, 11064. (n) van der Poll, T. S.; Love, J. A.; Nguyen, T. Q.; Bazan, G. C. *Adv. Mater.* **2012**, *24*, 3646.

(10) (a) Roquet, S.; Cravino, A.; Leriche, P.; Alévêque, O.; Frère, P.; Roncali, J. *J. Am. Chem. Soc.* **2006**, *128*, 3459. (b) Xia, P. F.; Feng, X. J.; Lu, J.; Tsang, S.-W.; Movileanu, R.; Tao, Y.; Wong, M. S. *Adv. Mater.* **2008**, *20*, 4810. (c) Kronenberg, N. M.; Deppisch, M.; Würthner, F.; Lademann, H. W. A.; Deing, K.; Meerholz, K. *Chem. Commun.* **2008**, 6489. (d) Bürckstümmer, H.; Kronenberg, N. M.; Gsänger, M.; Stolte, M.; Meerholz, K.; Würthner, F. *J. Mater. Chem.* **2010**, *20*, 24. (e) Kronenberg, N. M.; Steinmann, V.; Bürckstümmer, H.; Hwang, J.; Hertel, D.; Würthner, F.; Meerholz, K. *Adv. Mater.* **2010**, *22*, 4193. (f) Würthner, F.; Meerholz, K. *Chem.—Eur. J.* **2010**, *16*, 9366. (g) Steinmann, V.; Kronenberg, N. M.; Lenze, M. R.; Graf, S. M.; Hertel, D.; Meerholz, K.; Bürckstümmer, H.; Tulyakova, E. V.; Würthner, F. *Adv. Energy Mater.* **2011**, *1*, 888. (h) Bürckstümmer, H.; Tulyakova, E. V.; Deppisch, M.; Lenze, M. R.; Kronenberg, N. M.; Gsänger, M.; Stolte, M.; Meerholz, K.; Würthner, F. *Angew. Chem., Int. Ed.* **2011**, *123*, 11832.

(11) (a) Xue, J.; Uchida, S.; Rand, B. P.; Forrest, S. R. *Appl. Phys. Lett.* **2004**, *85*, 5757. (b) Drechsel, J.; Männig, B.; Kozlowski, F.; Pfeiffer, M.; Leo, K.; Hoppe, H. *Appl. Phys. Lett.* **2005**, *86*, 244102.

(12) (a) Scharber, M. C.; Mühlbacher, D.; Koppe, M.; Denk, P.; Waldauf, C.; Heeger, A. J.; Brabec, C. J. *Adv. Mater.* **2006**, *18*, 789. (b) Dennler, G.; Scharber, M. C.; Ameri, T.; Denk, P.; Forberich, K.; Waldauf, C.; Brabec, C. J. *Adv. Mater.* **2008**, *20*, 579.

(13) http://www.heliatek.com; Heliatek GmbH: Dresden, Germany.

(14) (a) Lin, L.-Y.; Tsai, C.-H.; Wong, K.-T.; Huang, T.-W.; Wu, C.-C.; Chou, S.-H.; Lin, F.; Chen, S.-H.; Tsai, A.-I. *J. Mater. Chem.* **2011**, *21*, 5950. (b) Lin, L.-Y.; Tsai, C.-H.; Lin, F.; Huang, T.-W.; Chou, S.-H.; Wu, C.-C.; Wong, K.-T. *Tetrahedron* **2012**, *68*, 7509.

(15) (a) Lin, L.-Y.; Chen, Y.-H.; Huang, Z.-Y.; Lin, H.-W.; Chou, S.-H.; Lin, F.; Chen, C.-W.; Liu, Y.-H.; Wong, K.-T. *J. Am. Chem. Soc.* **2011**, *133*, 15822. (b) Chiu, S.-W.; Lin, L.-Y.; Lin, H.-W.; Chen, Y.-H.; Huang, Z.-Y.; Lin, Y.-T.; Lin, F.; Liu, Y.-H.; Wong, K.-T. *Chem. Commun.* **2012**, *48*, 1857.

(16) (a) Casado, J.; Pappenfus, T. M.; Miller, L. L.; Mann, K. R.; Ortí, E.; Viruela, P. M.; Pou-AméRigo, R.; Hernández, V.; López Navarrete, J. T. *J. Am. Chem. Soc.* **2003**, *125*, 2524. (b) Pai, C.-L.; Liu, C.-L.; Chen, W.-C.; Jenekhe, S. A. *Polymer* **2006**, *47*, 699.

(17) (a) Tammer, M.; Monkman, A. P. *Adv. Mater.* **2002**, *14*, 210. (b) Lin, H.-W.; Lin, C.-L.; Chang, H.-H.; Lin, Y.-T.; Wu, C.-C.; Chen, Y.-M.; Chen, R.-T.; Chien, Y.-Y.; Wong, K.-T. *J. Appl. Phys.* **2004**, *95*, 881. (c) Lin, H.-W.; Lin, C.-L.; Wu, C.-C.; Chao, T.-C.; Wong, K.-T. *Org. Electron.* **2007**, *8*, 189.

(18) (a) Ng, A. M. C.; Cheung, K. Y.; Fung, M. K.; Djurišić, A. B.; Chan, W. K. *Thin Solid Films* **2008**, *517*, 1047. (b) Djurišić, A. B.; Fritz, T.; Leo, K. *J. Opt. A: Pure Appl. Opt.* **2000**, *2*, 458.

(19) Lin, H.-W.; Lin, L.-Y.; Chen, Y.-H.; Chen, C.-W.; Lin, Y.-T.; Chiu, S.-W.; Wong, K.-T. *Chem. Commun.* **2011**, *47*, 7872.

(20) Lin, L.-Y.; Lu, C.-W.; Huang, W.-C.; Chen, Y.-H.; Lin, H.-W.; Wong, K.-T. *Org. Lett.* **2011**, *13*, 4962.

(21) (a) Shrotriya, V.; Li, G.; Yao, Y.; Moriarty, T.; Emery, K.; Yang, Y. *Adv. Funct. Mater.* **2006**, *16*, 2016. (b) Snaith, H. J. *Energy Environ. Sci.* **2012**, *5*, 6513.

(22) Yang, L.; Zhang, T.; Zhou, H.; Price, S. C.; Wiley, B. J.; You, W. *ACS Appl. Mater. Interfaces* **2011**, *3*, 4075.

(23) Kim, M.-S.; Kim, B.-G.; Kim, J. *ACS Appl. Mater. Interfaces* **2009**, *1*, 1264.

(24) Koster, L. J. A.; Mihailetchi, V. D.; Blom, P. W. M. *Appl. Phys. Lett.* **2006**, *88*, 052104.

(25) (a) Chen, W.; Xu, T.; He, F.; Wang, W.; Wang, C.; Strzalka, J.; Liu, Y.; Wen, J.; Miller, D. J.; Chen, J.; Hong, K.; Yu, L.; Darling, S. B. *Nano Lett.* **2011**, *11*, 3707. (b) Collins, B. A.; Gann, E.; Guignard, L.; He, X.; McNeill, C. R.; Ade, H. *J. Phys. Chem. Lett.* **2010**, *1*, 3160.

(26) (a) Wynands, D.; Levichkova, M.; Riede, M.; Pfeiffer, M.; Baeuerle, P.; Rentenberger, R.; Denner, P.; Leo, K. *J. Appl. Phys.* **2010**, *107*, 014517. (b) Wynands, D.; Levichkova, M.; Leo, K.; Uhrich, C.; Schwartz, G.; Hildebrandt, D.; Pfeiffer, M.; Riede, M. *Appl. Phys. Lett.* **2010**, *97*, 073503.